Supporting Information

High Performance Two-Dimensional Perovskite $Ca_2Nb_3O_{10}$ UV Photodetectors

*Yong Zhang, Siyuan Li, Ziliang Li, Hui Liu, Xinya Liu, Jiaxin Chen, and Xiaosheng Fang**

Department of Materials Science, Fudan University, Shanghai 200433, P. R. China.

Corresponding Author

* E-mail: xshfang@fudan.edu.cn

This PDF file includes: Supplementary Text

Figure S1. (a) XPS survey spectrum of $Ca_2Nb_3O_{10}$ nanosheets. (b-d) High-resolution XPS spectra for elements Ca, Nb and O.

Figure S2. TEM image of the $Ca_2Nb_3O_{10}$ nanosheets.

Figure S3. Valence band XPS spectrum of the $Ca_2Nb_3O_{10}$ nanosheets.

Figure S4. Raman spectrum of the $Ca_2Nb_3O_{10}$ nanosheets.

Figure S5. Thermogravimetric analysis and differential scanning calorimetry curves of the $Ca_2Nb_3O_{10}$ nanosheets.

Figure S6. AFM image of the $Ca_2Nb_3O_{10}$ single photodetector and its corresponding height profile.

Figure S7. The schematic illustration of the $Ca_2Nb_3O_{10}$ nanosheets film photodetector.

Figure S8. The photograph of the flexible $Ca_2Nb_3O_{10}$ nanosheets film photodetector.

Figure S9. Energy band diagrams of the $Ca_2Nb_3O_{10}$ nanosheets film device taking into consideration of small Schottky barriers at the electrodes/channel contacts.

Figure S10. Top (a) and side (b) view of the optimized structures in DFT calculations for monolayer $HCa_2Nb_3O_{10}$.

Figure S11. Total electron density distribution (a) and charge density distribution (b) for monolayer $HCa_2Nb_3O_{10}$.

Figure S12. Calculated band structure (a) and total density of states (b) for monolayer $HCa_2Nb_3O_{10}$.

Table S1. Comparison of the main parameters for CNO nanosheets film photodetector and other pure material UV photodetectors in literature.

Table S2. Comparison of the main parameters for CNO nanosheets film photodetector and other composite materials UV photodetectors in literature.

REFERENCES S1-S33

Additional Figures

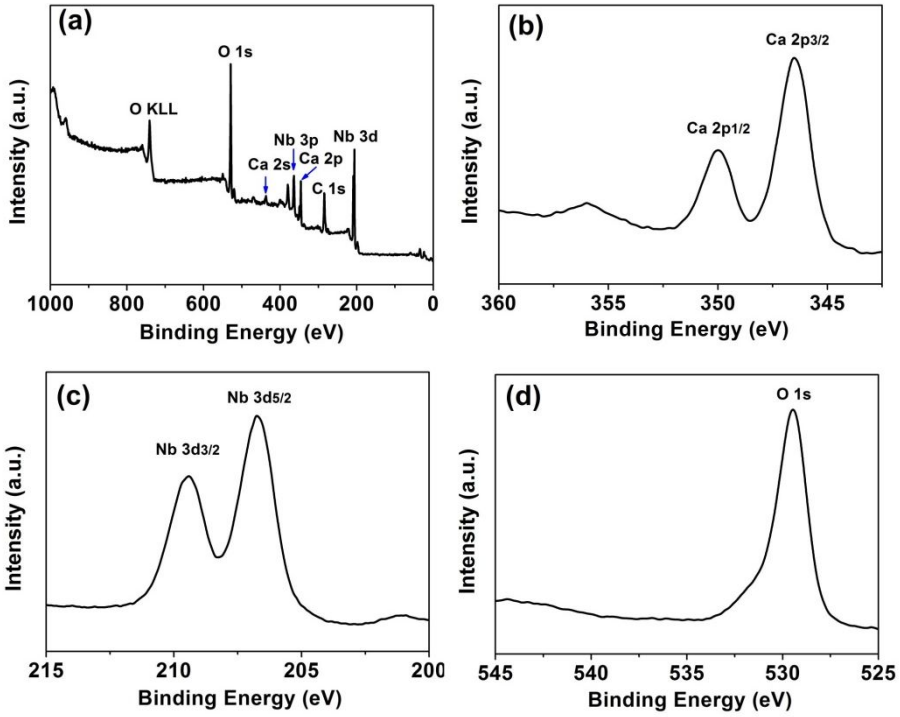

Figure S1. (a) XPS survey spectrum of $Ca_2Nb_3O_{10}$ nanosheets. (b-d) High-resolution XPS spectra for elements Ca, Nb and O.

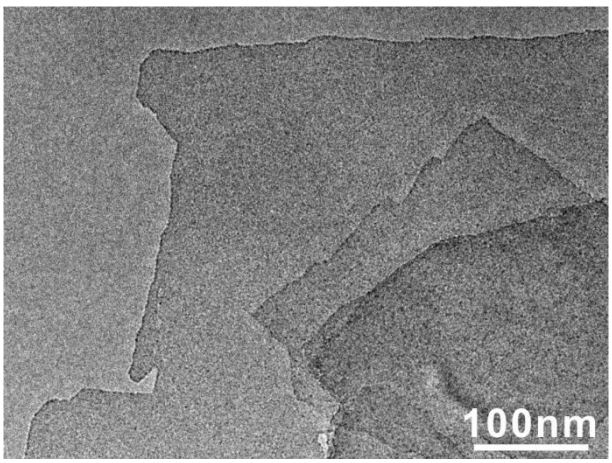

Figure S2. TEM image of the $Ca_2Nb_3O_{10}$ nanosheets.

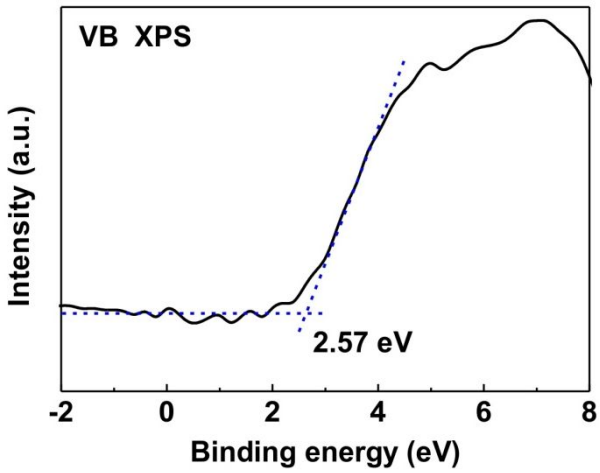

Figure S3. Valence band XPS spectrum of the $Ca_2Nb_3O_{10}$ nanosheets.

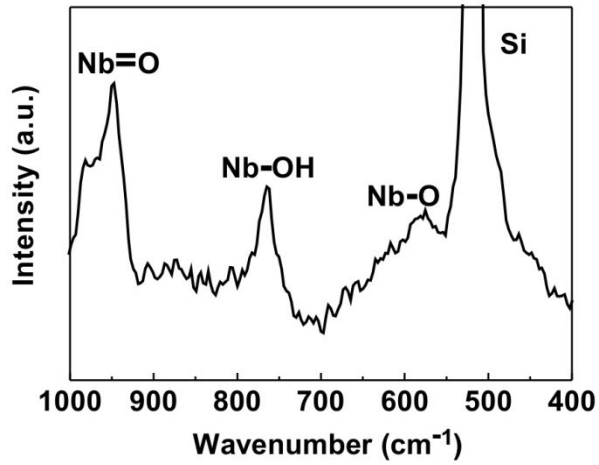

Figure S4. Raman spectrum of the $Ca_2Nb_3O_{10}$ nanosheets.

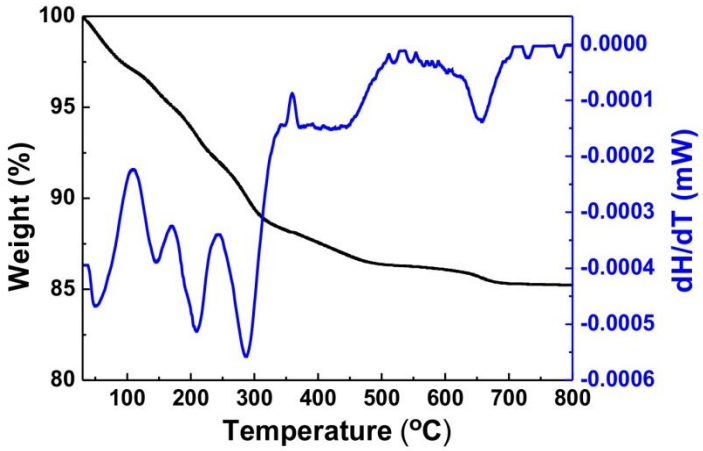

Figure S5. Thermogravimetric analysis and differential scanning calorimetry curves of the $Ca_2Nb_3O_{10}$ nanosheets.

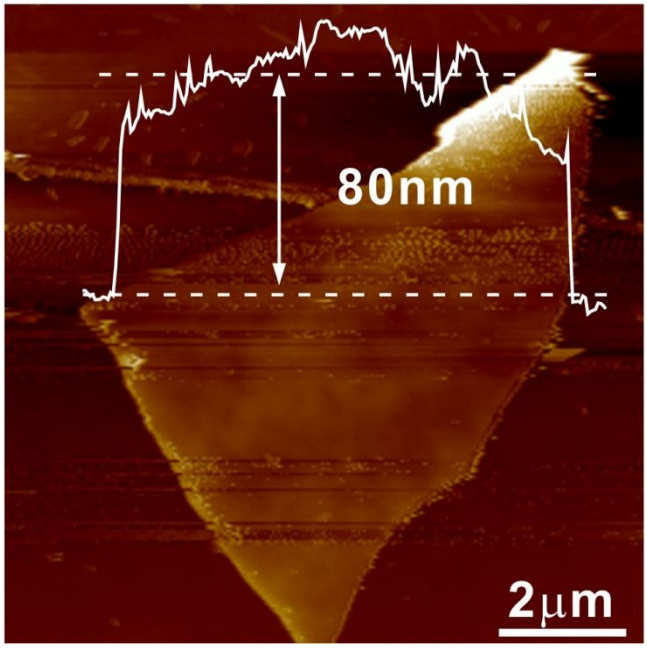

Figure S6. AFM image of the $Ca_2Nb_3O_{10}$ single photodetector and its corresponding height profile.

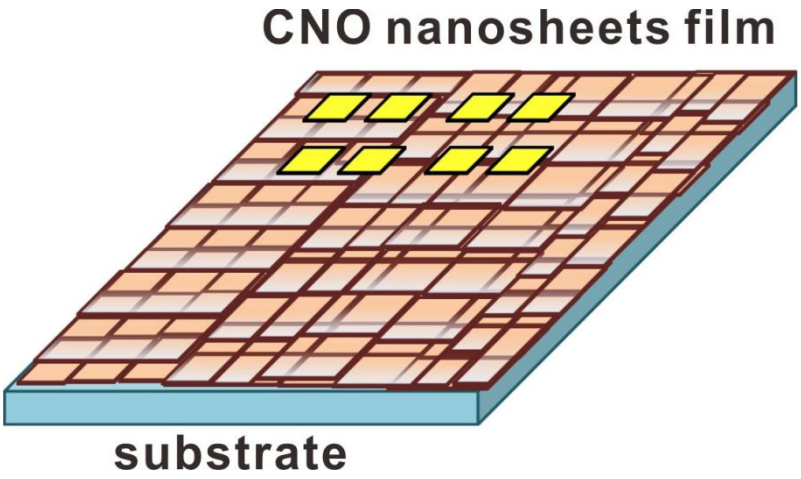

Figure S7. The schematic illustration of the $Ca_2Nb_3O_{10}$ nanosheets film photodetector.

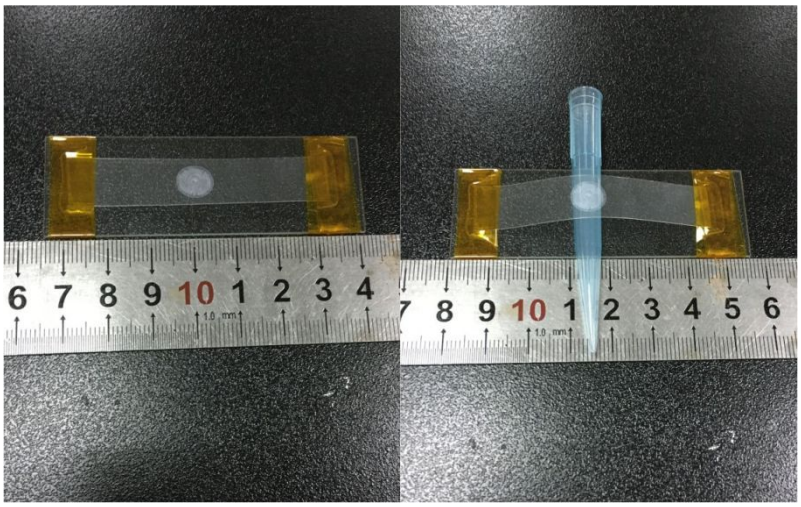

Figure S8. The photograph of the flexible $Ca_2Nb_3O_{10}$ nanosheets film photodetector.

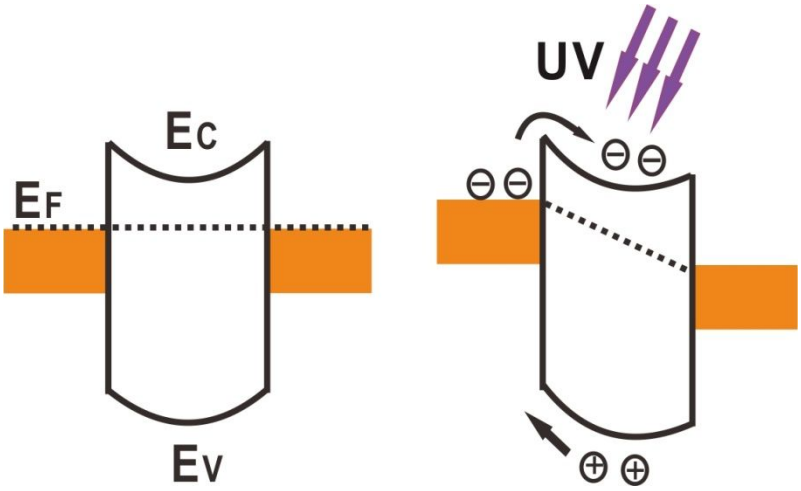

Figure S9. Energy band diagrams of the $Ca_2Nb_3O_{10}$ nanosheets film device taking into consideration of small Schottky barriers at the electrodes/channel contacts.

Material calculations

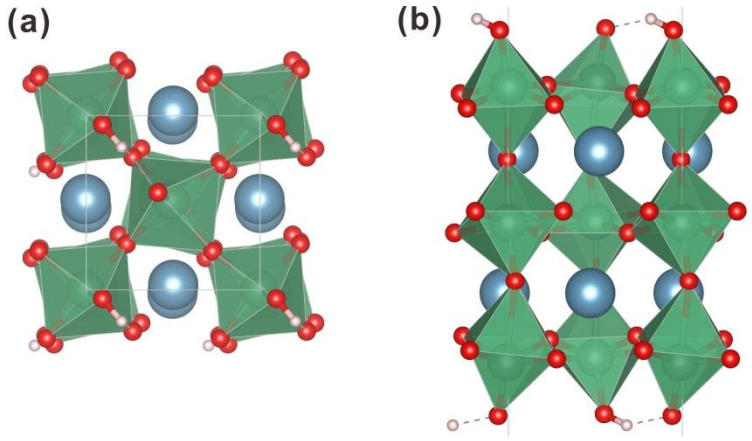

Figure S10. Top (a) and side (b) view of the optimized structures in DFT calculations for monolayer $HCa_2Nb_3O_{10}$.

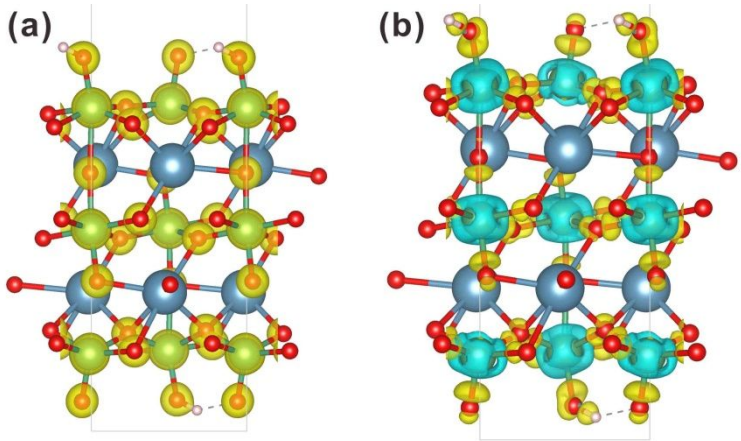

Figure S11. Total electron density distribution (a) and charge density distribution (b) for monolayer $HCa_2Nb_3O_{10}$.

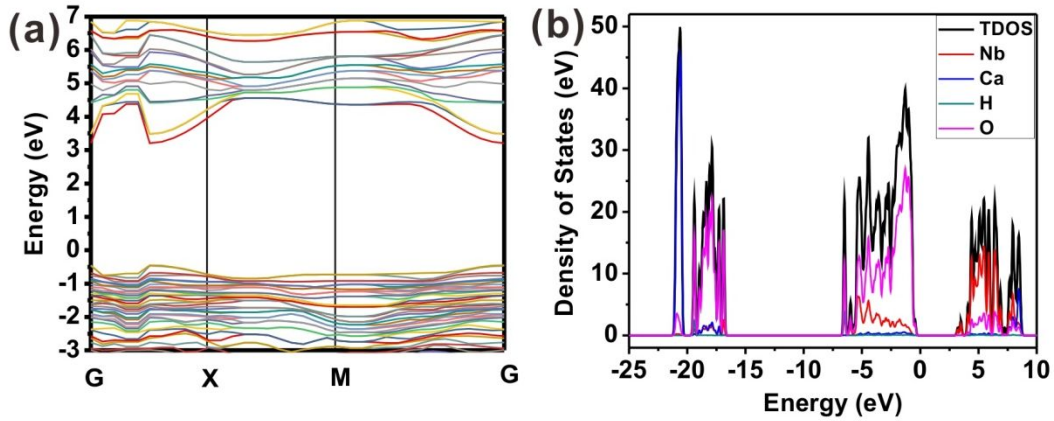

Figure S12. Calculated band structure (a) and total density of states (b) for monolayer $HCa_2Nb_3O_{10}$.

Table S1. Comparison of the main parameters for CNO nanosheets film photodetector and other pure material UV photodetectors in literature.

Materials	Methods	Nm (V)	R (I_{ph})	D*(Jones) (On-off)	T_r/T_d	Flexible	Ref.
TiO_2 nanotube	Electrochemical Anodization	312nm (2.5V)	13A/W –	– ($\sim10^4$)	0.5/0.7s	No	[S1]
TiO_2 film	Sol-gel Spin-coating	260nm (5V)	199A/W –	– ($\sim10^3$)	6/15s	No	[S2]
ZnO film	Fame-spray-pyrolysis	370nm (5V)	12A/W (1.2mA)	– ($3.3*10^5$)	250/150s	No	[S3]
ZnO nanowires	Vapor-liquid-solid process	360nm (1V)	0.39A/W (34nA)	$1.9*10^8$ (12)	2/100s	No	[S4]
SnO_2 nanowire	Glancing angle deposition	310nm (2V)	0.142A/W (19nA)	$10.8*10^{10}$ (1.34)	0.18/0.25s	No	[S5]
β-Ga_2O_3 flake	Mechanical exfoliation	254nm (10V)	29.8A/W –	$1.45*10^{12}$ (10^4)	>1/1s	No	[S6]
GaN film	electro-chemical-tchin g	340nm (1V)	10^4A/W –	$5.3*10^{14}$ –	>20/60s	No	[S7]
SiC film	Laser plasma deposition	250nm (10V)	0.18A/W –	– –	>14/60s	No	[S8]
ZnS nanobelts	Chemical vapor deposition	320nm (20V)	– (1.0nA)	– ($\sim10^3$)	2.57/1.99ms	No	[S9]
BiOCl film	Chemical bath method	350nm (5V)	0.76μA/W (34.7pA)	– (1.7)	1.03/10.6s	No	[S10]
MgZnO nanorod	RF magnetron sputtering	350nm (1V)	0.59mA/W –	2.7×10^6 –	30.9/39.7s	No	[S11]
BeZnO film	Molecular beam epitaxy	325nm (5V)	25mA/W (0.4nA)	$4*10^9$ –	1.48/4ms	No	[S12]
Zn_2SnO_4 nanowire	Thermal evaporation	254nm (20V)	– (138 nA)	– (10^4)	0.46/0.42s	No	[S13]
Zn_2GeO_4 nanowires	Vapor-liquid-solid	254nm (20V)	– (0.2 nA)		0.3/0.2s	No	[S14]
$Ga_2In_4S_9$ flakes	Chemical vapor deposition	360nm (5V)	111.9A/W (100nA)	$2.25*10^{11}$ ($2.1*10^3$)	40/50ms	No	[S15]
CuBr flakes	Chemical vapor deposition	345nm (10V)	3.17A/W (12pA)	$1.4*10^{11}$ –	48/32ms	No	[S16]
Nb_2O_5 nanobelt	Topochemical process	320nm (1V)	24.7A/W (50pA)	– –	28/12s	No	[S17]
$K_2Nb_8O_{21}$ nanowire	Molten salt sintering	320nm (5V)	2.53A/W (13.5pA)	– –	<0.3/0.3s	No	[S18]
$Ca_2Nb_3O_{10}$	**Calcination**	**300nm**	**14.94A/W**	**$8.7*10^{13}$**	**0.08/5.6ms**	**Yes**	**This**

nanosheets	**exfoliation**	**(3V)**	**(620nA)**	**($3.4*10^4$)**			**work**

Table S2. Comparison of the main parameters for CNO nanosheets film photodetector and other composite materials UV photodetectors in literature.

Materials	**Methods**	**Nm (V)**	**R/ (I_{ph})**	**D*/ (On-off)**	**T_r/T_d**	**Flex-ible**	**Ref.**
TiO_2-BiOCl Tube/nanosheets	Anodization-impregnation	350nm (5V)	41.9A/W –	$1.4*10^{14}$ ($2.2*10^5$)	12.9/0.8s	No	[S19]
ZnO film-**Cu** nanowires	Spin-coating	350nm (1V)	– (2.95nA)	– (98)	10.35/2s	No	[S20]
ZnO:graphdiyne film	Spin-coating	365nm (10V)	1260A/W –	– ($\sim10^5$)	6.1/2.1s	No	[S21]
SnO_2-ZnO nanofibers	Electrospinning	300nm (10V)	– (7.9nA)	– (4.6×10^3)	32.2/7.8 s	No	[S22]
SnO_2-Zn_2SnO_4 nanoparticle film	Drop-casting/ annealing	310nm (5V)	0.52A/W –	– ($\sim10^3$)	0.78/0.82s	No	[S23]
Ga_2O_3-ZnO heterostructures	Chemical vapor deposition	254nm (-2V)	11.1A/W (4.5μA)	– –	0.1/0.6ms	No	[S24]
GaN-Ga_2O_3 p-n junction	Pulse laser deposition	365nm (2V)	182mA/W –	$6.17*10^{10}$ –	0.15/0.12s	No	[S25]
3C-SiC/Si heterostructure	Chemical vapor deposition	375nm (2V)	3.2mA/W –	$1.8*10^6$ –	0.32/0.36s	No	[S26]
p-MgZnO/n-Si heterojunction	Dual Ion Beam Sputtering	310nm (1V)	25mA/W –	$8.91*10^{10}$ –	0.1/0.1s	No	[S27]
ZnS/ZnO biaxial nanobelt	Thermal evaporation	320nm (5V)	– (4.64μA)	– (6.9)	03/1.7s	No	[S28]
graphene/β-**Ga_2O_3**/graphene	metal organic chemical vapor deposition	254nm (5V)	1.05A/W –	– ($3.3*10^5$)	4.5/2.2s	No	[S29]
graphene/**InGaN**/graphene	Molecular beam epitaxy	380nm (5V)	$2.7*10^4$A/W –	– ($3*10^4$)	47/71μs	No	[S30]
$CsPbBr_3$/perovskite photodiode	Solution-Spin-coating	279nm (-0.1V)	1.4mA/W –	$2.4*10^{11}$ –	<70/70ms	No	[S31]
AZO/**ZnO/PVK**/PEDOT:PSS	Magnetron sputtering	365nm (5V)	81.6 mA/W –	$3.5*10^9$ –	0.11/0.2s	Yes	[S32]
$CsPbBr_3$ films	Spin-coating	254nm (2V)	0.24mA/W –	$1*10^{10}$ (10^3)	0.26/0.28s	Yes	[S33]
$Ca_2Nb_3O_{10}$ nanosheets	**calcination exfoliation**	**300nm (3V)**	**14.94A/W (620nA)**	**$8.7*10^{13}$ ($3.4*10^4$)**	**0.08/5.6 ms**	**Yes**	**This work**

REFERENCES

S1. Zou, J.; Zhang, Q.; Huang, K.; Marzari, N. Ultraviolet photodetectors based on anodic TiO_2 nanotube arrays, *J. Phys. Chem. C* **2010**, *114*(24), 10725-10729.

S2. Xue, H.; Kong, X.; Liu, Z.; Liu, C.; Zhou, J.; Chen, W. TiO_2 based metal-semiconductor-metal ultraviolet photodetectors, *Appl. Phys. Lett.* **2007**, *90*(20), 201118.

S3. Nasiri, N.; Bo, R.; Wang, F.; Fu, L.; Tricol, A. Ultraporous electron-depleted ZnO nanoparticle networks for highly sensitive portable visible-blind UV photodetectors, *Adv. Mater.* **2015**, *27*(29), 4336-4343.

S4. Weng, W.; Chang, S.; Hsu, C.; Hsueh, T.; Chang, P. A lateral ZnO nanowire photodetector prepared on glass substrate, *J. Electrochem. Soc.* **2010**, *157*(2), K30-K33.

S5. Chetri, P.; Dhar, J. Au/GLAD-SnO_2 nanowire array-based fast response Schottky UV detector, *Appl. Phys. A.* **2019**, *125*(5), 286.

S6. Oh, S.; Kim, C.; Kim, J. High responsivity β-Ga_2O_3 metal−semiconductor−metal solar-blind photodetectors with ultraviolet transparent graphene electrodes, *ACS Photonics* **2018**, *5*(3), 1123-1128.

S7. Liua, L.; Yang, C.; Patanè, A.; Yu, Z.; Yan, F.; Wang, K.; Lu, H.; Li, J.; Zhao, L. High-detectivity ultraviolet photodetectors based on laterally mesoporous GaN, *Nanoscale*, **2017**, *9*(24), 8142-8148.

S8. Aldalbahi, A.; Li, E.; Rivera, M.; Velazquez, R.; Altalhi, T.; Peng, X.; Feng, P. A new approach for fabrications of SiC based photodetectors, *Sci. Rep*. **2016**, *6*, 23457.

S9. Fang, X.; Bando, Y.; Liao, M.; Zhai, T.; Gautam, U.; Li, L.; Koide, Y.; Golberg, D. An efficient way to assemble ZnS nanobelts as ultraviolet-light sensors with enhanced photocurrent and stability, *Adv. Funct. Mater*. **2010**, *20*(3), 500-508.

S10. Ouyang, W.; Su, L.; Fang, X. UV photodetectors based on BiOCl nanosheet arrays: the effects of morphologies and electrode configurations, *Small* **2018**, *14*(36), 1801611.

S11. Young, S.; Liu, Y. Low-frequency noise properties of MgZnO nanorod ultraviolet photodetectors with and without UV illumination, *Sens. Actuators. A* **2018**, *269*, 363-369.

S12. Su, L.; Zhu, Y.; Xu, X.; Chen, H.; Tang, Z.; Fang, X. Back-to-back symmetric schottky type UVA photodetector based on ternary alloy BeZnO, *J. Mater. Chem. C.* **2018**, *6*(29), 7776-7782.

S13. Zhang, Y.; Wang, J.; Zhu, H.; Li, Jiang, L.; Shu, C.; Hua, W.; Wang, C. High performance ultraviolet photodetectors based on an individual Zn_2SnO_4 single crystalline nanowire, *J. Mater. Chem*. **2010**, *20*(44), 9858-9860.

S14. Yan, Y.; Singh, N.; Lee, P. Wide-bandgap Zn_2GeO_4 nanowire networks as efficient ultraviolet photodetectors with fast response and recovery time, *Appl. Phys. Lett*. **2010**, *96*(5), 053108.

S15. Wang, F.; Gao, T.; Zhang, Q.; Hu, Z.; Jin, B.; Li, L.; Zhou, X.; Li, H.; Tendeloo, G.; Zhai, T. Liquid-alloy-assisted arowth of 2D ternary $Ga_2In_4S_9$ toward high-performance UV photodetection, *Adv. Mater.* **2019**, *31*(2), 1806306.

S16. Gong, C.; Chu, J.; Yin, C.; Yan, C.; Hu, X.; Qian, S.; Hu, Y.; Hu, K.; Huang, J.; Wang, H.; Wang, Y.; Wangyang, P.; Lei, T.; Dai, L.; Wu, C.; Chen, B.; Li, C.; Liao, M.; Zhai, T.; Xiong, J. Self-confined growth of ultrathin 2D nonlayered wide-bandgap semiconductor CuBr flakes, *Adv. Mater.* **2019**, *31*(36), 1903580.

S17. Liu, H.; Gao, N.; Liao, M.; Fang, X. Hexagonal-like Nb_2O_5 nanoplates-based photodetectors and photocatalyst with high performances, *Sci. Rep*. **2015**, *5*, 7716.

S18. Liu, H.; Zhang, Z.; Hu, L.; Gao, N.; Sang, L.; Liao, M.; Ma, R.; Xu, F.; Fang, X. New UV-A photodetector based on individual potassium niobate nanowires with high performance, *Adv. Optical Mater.* **2014**, *2*(8), 771-778.

S19. Ouyang, W.; Teng, F.; Fang, X. High performance BiOCl nanosheets/TiO_2 nanotube arrays heterojunction UV photodetector: the influences of self-induced inner electric fields in the BiOCl nanosheets, *Adv. Funct. Mater.* **2018**, *28*(16), 1707178.

S20. Teng, F.; Zheng, L.; Hu, K.; Chen, H.; Li, Y.; Zhang, Z.; Fang, X. A surface oxide thin layer of copper nanowires enhanced the UV selective response of a ZnO film photodetector, *J. Mater. Chem. C.* **2016**, *4*(36), 8416-8421.

S21. Jin, Z.; Zhou, Q.; Chen, Y.; Mao, P.; Li, H.; Liu, H.; Wang, J.; Li, Y. Graphdiyne:ZnO nanocomposites for high-performance UV photodetectors, *Adv. Mater.* **2016**, *28*(19), 3697-3702.

S22. Tian, W.; Zhai, T.; Zhang, C.; Li, S.; Wang, X.; Liu, F.; Liu, D.; Cai, X.; Tsukagoshi, K.; Golberg, D.; Bando, Y. Low-cost fully transparent ultraviolet photodetectors based on electrospun ZnO-SnO_2 heterojunction nanofibers, *Adv. Mater.* **2013**, *25*(33), 4625-4630.

S23. Liu, C.; Piyadasa, A.; Piech, M.; Dardona, S.; Rena, Z.; Gao, P. Tunable UV response and high performance of zinc stannate nanoparticle film photodetectors, *J. Mater. Chem. C.* **2016**, *4*(25), 6176-6184.

S24. Zhao, B.; Wang, F.; Chen, H.; Zheng, L.; Su, L.; Zhao, D.; Fang, X. An ultrahigh responsivity (9.7 mA W^{-1}) self-powered solar-blind photodetector based on individual ZnO-Ga_2O_3 heterostructures, *Adv. Funct. Mater.* **2017**, *27*(17), 1700264.

S25. Li, P.; Shi, H.; Chen, K.; Guo, D.; Cui, W.; Zhi, Y.; Wang, S.; Wu, Z.; Chenb, W.; Tang, W. Construction of GaN/Ga_2O_3 p-n junction for an extremely high responsivity self-powered UV photodetector, *J. Mater. Chem. C.* **2017**, *5*(40), 10562-10570.

S26. Md Foisal, A.; Dinh, T.; Tanner, P.; Phan, H.; Nguyen, T.; Streed, E.; Viet Dao, D. Photoresponse of a highly-rectifying 3C-SiC/Si heterostructure under UV and visible illuminations, *IEEE Electr. Device. L.* **2018**, *39*(8), 1219-1222.

S27. Bhardwaj, R.; Sharma, P.; Singh, R.; Mukherjee, S. Sb-doped *p*-MgZnO/*n*-Si heterojunction UV photodetector fabricated by dual ion beam sputtering, I*EEE Photonic Tech. L.* **2017**, *29*(14), 1215-1218.

S28. Hu, L.; Yan, J.; Liao, M.; Xiang, H.; Gong, X.; Zhang, L.; Fang, X. An optimized ultraviolet-A light photodetector with wide-range photoresponse based on ZnS/ZnO biaxial nanobelt, *Adv. Mater.* **2012**, *24*(17), 2305-2309.

S29. Li, Y.; Zhang, D.; Lin, R.; Zhang, Z.; Zheng, W.; Huang, F. Graphene interdigital electrodes for improving sensitivity in a Ga_2O_3:Zn deep-ultraviolet photoconductive detector, *ACS Appl. Mater. Interfaces* **2019**, *11*(1), 1013-1020.

S30. Zheng, Y.; Wang, W.; Li, Y.; Lan, J.; Xia, Y.; Yang, Z.; He, X.; Li, G. Self-integrated hybrid ultraviolet photodetectors based on the vertically aligned InGaN nanorod array assembly on graphene, *ACS Appl. Mater. Interfaces* **2019**, *11*(14), 13589-13597.

S31. Zou, T.; Liu, X.; Qiu, R.; Wang, Y.; Huang, S.; Liu, C.; Dai, Q.; Zhou, H. Enhanced UV-C detection of perovskite photodetector arrays via inorganic $CsPbBr_3$ quantum dot down-conversion layer, *Adv. Optical Mater.* **2019**, *7*(11), 1801812.

S32. Zhang, X.; Li, J.; Yang, W.; Leng, B.; Niu, P.; Jiang, X.; Liu, B. High-performance flexible ultraviolet photodetectors based on AZO/ZnO/PVK/PEDOT:PSS heterostructures integrated on human hair, *ACS Appl. Mater. Interfaces* **2019**, *11*(27), 24459-24467.

S33. Zhang, T.; Wang, F.; Zhang, P.; Wang, Y.; Chen, H.; Li, J.; Wu, J.; Chen, L.; Chen, Z.; Li, S. Low-temperature processed inorganic perovskites for flexible detectors with a broadband photoresponse, *Nanoscale*, **2019**, *11*(6), 2871-2877.